To appear in *Phys. Rev. E*

Spatial heterogeneity and the stability of reaction states in autocatalysis

Glenn Marion*
Biomathematics & Statistics Scotland, James Clerk Maxwell Building, The King's Buildings, Mayfield Rd, Edinburgh, EH9 3JZ

Xuerong Mao, Eric Renshaw
Department of Statistics & Modelling Science, University of Strathclyde, Glasgow, G1 1XH

Junli Liu
Computational Biology Programme, Scottish Crop Research Institute, Invergowrie, Dundee, DD2 5DA, UK

The impact of stochasticity and spatial heterogeneity on the quadratic autocatalytic system is studied. In a nonspatial setting the reactive state of the system is found to be unstable in small volumes where internal fluctuations drive the system to the unreactive state. This phenomena is of potential importance to the stability of reactions in biological cells. A simple spatial model is constructed by linking N nonspatial models via migration of reactants controlled by a mixing rate λ. Simulation of this stochastic process demonstrates the importance of such mixing in controlling the impact of internal fluctuations on the stability of the autocatalytic reaction. For high mixing rate the mean reactant levels in equilibrium correspond to the well-mixed deterministic system, although a significant degree of spatial heterogeneity remains. For intermediate mixing rates, mean reactant levels vary continuously with λ where the interaction of internal fluctuations with limited spatial mixing modifies the reactive states of the deterministic system. However, there is a threshold below which mixing is unable to control internal fluctuations which drive the system into the unreactive state. Thus a critical minimum level of communication between the cells is required to stabilize the reaction across the entire system. Approximate analytic results, obtained using moment-closure techniques, support these findings and demonstrate the relationship between the spatial stochastic and nonspatial deterministic models.

PACS numbers: 82.39.-k,82.20.-w,02.50.-r
Keywords: internal fluctuations, Markov process, spatio-temporal stochastic processes, moment closure approximation, autocatalysis, noise induced transitions, biochemical reactions

I. INTRODUCTION

In the absence of macroscopic environmental fluctuations, classical reaction kinetics applies ordinary differential equations to describe the progress of reactions in large volumes under conditions of perfect mixing. However, in many biochemical systems reactions occur in minute volumes and both stochasticity and spatial heterogeneity play important roles in living cells. For example, by reference to cell volume Gibson and Bruck [1] show that the number of protein molecules involved in reactions controlling gene regulation in Lambda phage infection of *Escherichia coli* is of the order 10 to 100. Moreover, the outcome of this infection process is stochastic. Autocatalytic mechanisms play an important role in the organization and coordination of biological cells, and quadratic- or cubic-autocatalysis represent generic models whose behaviour in stochastic and spatially heterogeneous systems are important for understanding processes in living cells. This paper addresses these issues by exploring the impact of stochasticity and spatial heterogeneity in the quadratic autocatalytic process

$$A + B \to 2B \qquad B \to C\,,$$

where a B-particle catalyses the conversion of reactant A into further Bs, and reactant B also decays to product C [2, 3]. Positive feedback is seen as a central mechanism in many important biochemical processes such as glycolysis [4]; autocatalytic systems of this type have been widely studied as prototypical feedback systems [2, 3, 5, 6]. Horsthemke and Lefever [7] study the effect of environmental noise on a range of one-dimensional dynamical systems, and find that stochasticity may radically alter the behaviour of deterministic models, for example by inducing transitions between steady states of the deterministic system, altering the level of such states or by inducing new states. Marion *et. al.* [8] study the effect of both environmental and internal noise on the quadratic autocatalytic processes in the nonspatial setting of a continuous-flow stirred tank reactor (CSTR), whilst the present paper focuses on the role of internal fluctuations in a spatially extended system. First, however, we review the behaviour of the nonspatial process.

When quadratic autocatalysis is carried out in a CSTR the system can be considered to be well-mixed, of large volume and adequately described by the deterministic

*Contact email:glenn@bioss.ac.uk

model

$$\begin{aligned} d\alpha(t)/dt &= (\alpha_0 - \alpha(t))\,\nu - \kappa\,\alpha(t)\,\beta(t) \\ d\beta(t)/dt &= \kappa\,\alpha(t)\,\beta(t) - (K_b + \nu)\,\beta(t)\,, \end{aligned} \tag{1}$$

where $\alpha(t)$ and $\beta(t)$ represent the concentrations of A- and B-particles, respectively. Reactant A is supplied at rate $\nu\alpha_0$ from a reservoir of fixed concentration α_0: both A and B are removed from the reaction vessel at rates $\nu\,\alpha$ and $\nu\,\beta$, respectively. The decay $B \to C$ occurs at rate $K_b\,\beta$, and the name of the process derives from the quadratic rate, $\kappa\,\alpha\,\beta$, for the autocatalytic step $A + B \to 2B$. This system has two fixed points, the *reactive state* (α_1, β_1) and the *unreactive state* (α_2, β_2) given by

$$\begin{aligned} \alpha_1 &= (K_b + \nu)/\kappa,\ \beta_1 = \nu(\alpha_0\kappa - K_b - \nu)/(\kappa(K_b + \nu)) \\ \alpha_2 &= \alpha_0,\ \beta_2 = 0\,. \end{aligned} \tag{2}$$

Where chemical and biochemical reactions occur in small volumes, or in poorly mixed conditions, deterministic descriptions such as (1) prove inadequate, and this is particularly true at low densities where finite size effects are most significant. In such cases discrete state-space Markov models, or birth-death processes, have been extensively used in modelling chemical reactions and a wide range of biological and physical systems. In the physicochemical literature, models of this type are said to describe the state of the system at a *mesoscopic* scale: that is, an intermediate scale between the *microscopic*, where molecular dynamic or even quantum mechanical descriptions should be used, and the *macroscopic* scale where (in deterministic environments) deterministic descriptions such as (1) are often employed [9]. In a general birth-death process the probability of change of state in a small time interval $(t, t + \delta t)$ can be written

$$\mathrm{P}(n(t + \delta t) = n(t) + \delta n) = R(n \to n + \delta n)\delta t\,, \tag{3}$$

where the vector $\delta n = (\delta n_1, \delta n_2, ...)^T$ represents the change in state $n = (n_1, n_2, ...)^T$ which occurs at rate $R(n \to n + \delta n)$. The change δn_i in population i is an integer, and often ± 1. The fluctuations caused by the stochastic nature of the events are typically referred to as internal fluctuations in physical and chemical models, and as demographic fluctuations in biological systems. Whilst exact simulation is straightforward, since inter-event times are exponentially distributed [10], an approximate alternative approach is to update time by a sufficiently small time step δt and then to choose the event $n \to n + \delta n$ with probability (3).

To model the nonspatial quadratic autocatalytic system described above at the mesoscopic level, write $n = (n_A, n_B)^T$ with $\delta n = (\delta n_A, \delta n_B)^T$ and the rates $R(n \to n + \delta n)$ as

Rate	δn_A	δn_B	
Kn_An_B	-1	$+1$	Autocatalytic reaction
K_bn_B	0	-1	Decay of reactant B
νn_{A0}	$+1$	0	Influx of reactant A
νn_A	-1	0	Outflow of reactant A
νn_B	0	-1	Outflow of reactant B
0	otherwise.		

(4)

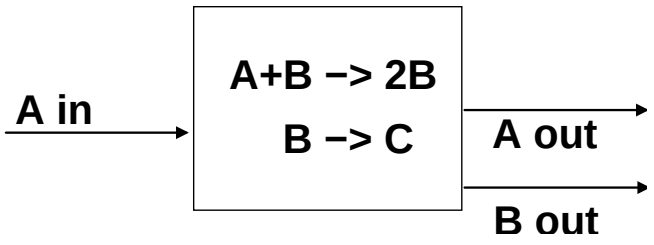

FIG. 1: Schematic representation of a nonspatial model of the autocatalytic process.

The connection with the deterministic system (1) is made by introducing the system volume Ω and writing the densities $\alpha = n_A/\Omega$ and $\beta = n_B/\Omega$, which for finite volumes are random variables. However, if the the reaction rate scales like $K = \kappa/\Omega$, then in the large volume limit $\Omega \to \infty$ it can be shown that α and β obey the deterministic equations (1) [8, 11, 12].

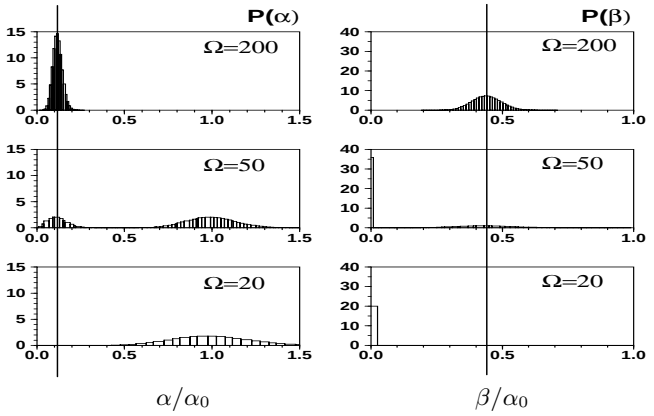

FIG. 2: The e ect of volume in the nonspatial system. Histograms from simulations of the Markov process (3)-(4), with $\alpha = n_A/$, $\beta = n_B/$, and parameter values $\kappa = 1$, $\alpha_0 = 1$, $\nu = K_b = 1/17$. Samples of the process are taken for $t = (900000, 1000000)$. The solid vertical lines represent the equilibrium values obtained from the deterministic model (1).

Figure 2 shows the effect of system volume on the stability of the reactive state. The results shown are based on simulated data collected for $t = (900000, 1000000)$ and thus represent samples from the quasi-equilibrium distribution of the birth-death process (3)-(4). The parameter values used are $\kappa = 1$, $\alpha_0 = 1$, $\nu = K_b = 1/17$ [5]. For large volume ($\Omega = 200$) internal fluctuations induce a distribution centered on the deterministic steady state (α_1, β_1); the reactive state is stable with respect to internal fluctuations. However, for small volumes ($\Omega = 20$) the system is driven toward an unreactive state with fluctuations about the deterministic steady state (α_2, β_2). At intermediate volumes ($\Omega = 50$) the reactive state remains stable with non-zero probability, but a proportion of realizations fall into the unreactive state. Thus, for small volumes, where the reactive state is totally destabilized

by internal fluctuations there are qualitative differences between deterministic and stochastic models. Zheng *et. al.* [13] study a related system in which the concentration of A-particles is held fixed. The exact stationary distribution may then be calculated since the resulting system is one-dimensional [10]. Zheng *et. al.* show that as the system volume increases the relative heights of peaks in this distribution invert; a similar effect to that shown in Figure 2. However, in contrast with the present case where only one fixed point of the deterministic dynamics is attracting, these peaks are associated with two attracting steady states of the corresponding deterministic system. For cellular systems it may seem un-natural to adjust system volume. However, the above results hold for changes in the density of reactants, with low densities corresponding to an unstable reactive state; for fixed cell volume changes in density correspond to changes in the number of reactant molecules per cell. Indeed, it has been found that in living cells the number of molecules can be very low and enzymatic reactions occur in small volumes [1, 14].

In the remainder of this paper we study the effect of spatial heterogeneity on the stability of the reactive state in quadratic autocatalysis. Section II introduces a spatial autocatalytic model in which N nonspatial processes (3)-(4), each with volume $\Omega = 1$, are coupled via random migration of B-particles which is controlled by a mixing rate λ. Stochastic simulation is used to explore the stability of the reactive state for a range of values of λ. Section III applies moment-closure techniques to develop approximations describing the system, they: support the simulation results; reveal the relationship between the nonspatial deterministic model and the spatial stochastic system; and yield analytic insights into system behaviour in the limits of high and low mixing. Finally, in section IV we discuss the relevance of our results to living cells.

II. SPATIAL PROCESS

Figure 3 depicts the spatial autocatalytic process constructed by linking N nonspatial models via the migration of B-particles. The numbers of A and B particles at site $i = 1, ..., N$ are denoted n_i^A and n_i^B, respectively. The within-site behaviour is described by the nonspatial model (3)-(4), whilst the migration of B-particles is described by

$$\begin{aligned} \mathrm{P}(n_i^B(t+\delta t) = n_i^B(t) - 1) &= \lambda n_i^B \delta t \\ \mathrm{P}(n_i^B(t+\delta t) = n_i^B(t) + 1) &= \frac{\lambda}{N} \sum_{j=1}^{N} n_j^B \delta t \,. \end{aligned} \tag{5}$$

where the first equation is the probability of migration from site i and the latter, that of migration to site i. The resulting model can therefore be described as quadratic autocatalysis with random mixing of B-particles between cells. In what follows the volume of each site is taken to be $\Omega = 1$, where the total system volume is then N, the reaction rate $K = \kappa$ and $n_{A0} = \alpha_0$.

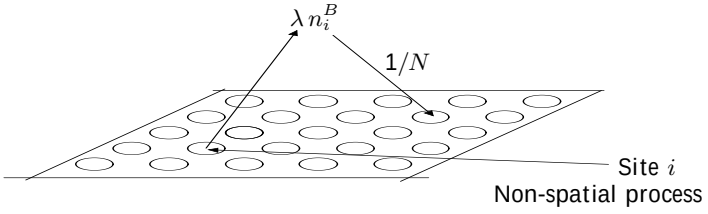

FIG. 3: Schematic representation of the spatial autocatalytic process in which N nonspatial Markov processes (3)-(4) are linked together via random migration of B-particles.

Consider the evolution of the average reactant levels

$$<n_A> \equiv \frac{1}{N} \sum_{i=1}^{N} n_i^A \quad \text{and} \quad <n_B> \equiv \frac{1}{N} \sum_{i=1}^{N} n_i^B \,.$$

Since we have set $\Omega = 1$, $<n_A>$ and $<n_B>$ are dimensionless quantities corresponding to the densitiesα and β respectively. Figure 4 shows these average reactant levels for typical realizations of the spatial process at two mixing rates. The results show that for small mixing rate $\lambda = 0.01$ the reactive state is unstable just as in the nonspatial model. However, a moderate mixing rate $\lambda = 1$ stabilizes the reactive state.

Figure 5 shows equilibrium estimates of the expected average reactant levels for a range of mixing rates $\lambda \in [0, 2]$. These results show that a critical minimum level of mixing is required to stabilize the reactive state. For small λ the mixing is insufficient to stabilize the reaction against stochastic fluctuation. However, as the rate of mixing increases, at some critical point the reaction becomes stable across the system. Communication allows the cells to act coherently. Moreover, just above this threshold, the density of the reaction product B is considerably lower than predicted by equation (2), but this increases with the mixing rate to an asymptote at the level of the well-mixed deterministic system. Thus one can think of λ as controlling the effective noise level: for small noise (large λ) the system is well mixed and the mean reactant levels coincide with the deterministic nonspatial model predictions; for intermediate levels of noise the reactive state is shifted with respect to the well mixed case; and for large noise (small λ) the reactive state is completely destabilized. Qualitatively similar results are obtained for small values of $\Omega \neq 1$.

III. SPATIAL MOMENT CLOSURE APPROXIMATION

In order to understand better the phenomena described above we derive analytic approximations describing the spatial system. In so doing we demonstrate the

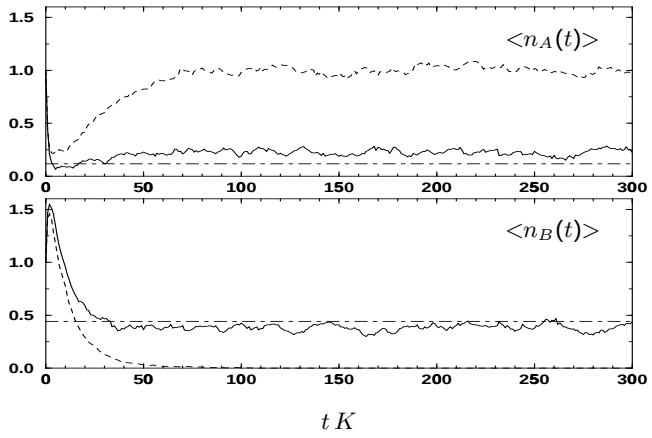

FIG. 4: **Simulation of spatial system:** The top graph shows typical realizations of the average density $< n_A(t) >$ from the stochastic spatial autocatalytic process described in Section II against dimensionless time tK for λ = 1 (solid curve) and λ = 0.01 (dashed curve). The bottom graph depicts the same information for reactant B. In each case the dot-dashed lines show the corresponding reactant levels obtained from deterministic equilibrium (2). The parameter values are K = 1, α_0 = 1, K_b = ν = 1/17 and N = 500.

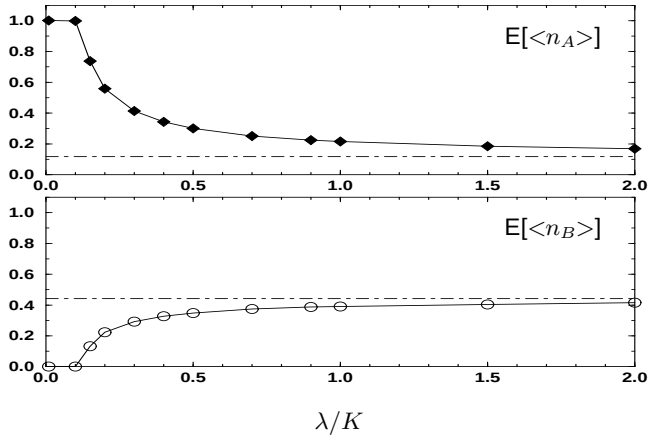

FIG. 5: **Stability of reaction state:** The symbols and solid curves represent estimates of E[$<n_A>$] (diamonds) and E[$<n_B>$] (circles) obtained from 10 simulation runs, with samples collected, after a burn-in period, from t = 500, ..., 1000, for a range of relative values of the mixing rateλ/K. The standard errors in these estimates are approximately equal to the size of the symbols. The dot-dashed lines show the corresponding reactant levels obtained from deterministic equilibrium (2). The parameter values are K = 1, α_0 = 1, K_b = ν = 1/17 and N = 500.

relationship between the deterministic nonspatial model and the stochastic spatial process. In particular, we construct equations describing the average reactant levels and apply the methodology developed by Keeling *et. al*, in the context of spatial models in ecology [15, 16]. This approach has two principal advantages over dealing directly with the site specific reactant levels, n_i^A and n_i^B. First, it reduces the dimensionality of the problem to be solved from $2N$ to 5 (see below). Second, even for moderate sized systems the variability of the average reactant levels will be much less than that of individual sites, and therefore the task of calculating associated statistics more straightforward.

Writing the change in the level of reactant A at site i as $n_i^A(t+\delta t) = n_i^A + \delta n_i^A$, the change in the average reactant level is

$$\frac{1}{N}\sum_{i=1}^{N} n_i^A(t+\delta t) = \frac{1}{N}\sum_{i=1}^{N} n_i^A + \frac{1}{N}\sum_{i=1}^{N} \delta n_i^A \,.$$

Using the transition probabilities for site i as defined in (3), (4) and (5), conditional on the state of the system at time t being $n = \{(n_1^A, ..., n_N^A)^T, (n_1^B, ..., n_N^B)^T\}$ the expected change during a small time interval $(t, t+\delta t)$ is then given by

$$\mathrm{E}\left[\frac{1}{N}\sum_{i=1}^{N} n_i^A(t+\delta t) \mid n(t) = n\right] =$$
$$\frac{1}{N}\sum_{i=1}^{N} n_i^A + \left(-\kappa\frac{1}{N}\sum_{i=1}^{N} n_i^A n_i^B + \nu\alpha_0 - \nu\frac{1}{N}\sum_{i=1}^{N} n_i^A\right)\delta t \,.$$

Whence evaluating expectations E[.] at time t, and rearranging, leads to

$$\mathrm{E}\left[\frac{1}{N}\sum_{i=1}^{N} n_i^A(t+\delta t)\right] - \mathrm{E}\left[\frac{1}{N}\sum_{i=1}^{N} n_i^A\right] =$$
$$\left(-\kappa\mathrm{E}\left[\frac{1}{N}\sum_{i=1}^{N} n_i^A n_i^B\right] + \nu\alpha_0 - \nu\mathrm{E}\left[\frac{1}{N}\sum_{i=1}^{N} n_i^A\right]\right)\delta t \,.$$

For any random variable z_i associated with site i, write the spatial average

$$<z> = \frac{1}{N}\sum_{i=1}^{N} z_i \,.$$

Then taking the limit $\delta t \to 0$ yields

$$\frac{d}{dt}\mathrm{E}[<n_A>] = -\kappa\mathrm{E}[<n_A n_B>] + \nu\alpha_0 - \nu\mathrm{E}[<n_A>] \,. \quad (6)$$

The equation describing the evolution of the average level of reactant B, namely

$$\frac{d}{dt}\mathrm{E}[<n_B>] = \kappa\mathrm{E}[<n_A n_B>] - (K_b + \nu)\mathrm{E}[<n_B>] \,, \quad (7)$$

is obtained in a similar manner. The difficulty with equations (6) and (7) is that they depend on the second-order term E[$<n_A n_B>$]. In order to close this system of equations one may choose to approximate this term as a function of the first-order terms E[$< n_A >$] and E[$< n_B >$]. This problem is characteristic of non-linear stochastic processes and a number of closure approximations exist. Broadly speaking, they may be classified into three

types, namely moment-closure, cumulant-truncation and spatial moment-closure. In each case higher-order terms such as $\mathrm{E}[<n_A n_B>]$ are replaced by functions of lower-order terms (i.e. $\mathrm{E}[<n_A>]$ and $\mathrm{E}[<n_B>]$). Moment-closure [17, 18] achieves this by making some ansatz which determines the functional dependence; for example that the process is Gaussian [19]. An alternative approach is cumulant-truncation [20, 21] whereby the moment equations are re-expressed in terms of cumulants (see e.g., 22) and higher-order cumulants are assumed to be zero. For example second-order cumulant truncation sets third- and higher-order cumulants to zero and thus corresponds to moment-closure by Normal approximation. The complexities involved in such methods are highlighted by the fact that higher-order truncation does not necessarily improve the accuracy of the approximation [23]. In spatial systems isotropy is often invoked and boundary (finite-size) effects are ignored. Attention then focuses entirely on spatial moments, and to eliminate higher-order terms one either makes a distributional assumption [15, 16] or appeals to the spatial connectedness of the system [24–26]. We note that closely related cluster approximations have been applied in chemical physics [27], and the study of non-ideal gases [28].

For the model considered here, the simplest moment-closure scheme is the *mean field* approximation which assumes that there is no correlation between the mean numbers of A and B particles, that is $\mathrm{E}[<n_A n_B>] = \mathrm{E}[<n_A>]\,\mathrm{E}[<n_B>]$. This recovers the deterministic system (1) on substituting $\alpha = \mathrm{E}[<n_A>]$ and $\beta = \mathrm{E}[<n_B>]$. However, to understand the effect of spatial heterogeneity, second-order terms must be considered. The following equations describing the evolution of $\mathrm{E}[<n_A n_B>]$, $\mathrm{E}[<n_A^2>]$ and $\mathrm{E}[<n_B^2>]$ can be developed along similar lines to equation (6):

$$\begin{aligned}
\frac{d}{dt}\mathrm{E}[<n_A n_B>] &= (\mathrm{E}[<n_A^2 n_B>] - \mathrm{E}[<n_A n_B^2>])\kappa \\
&\quad -(\kappa + K_b + 2\nu + \lambda)\mathrm{E}[<n_A n_B>] \\
&\quad +\lambda\mathrm{E}[<n_A><n_B>] + \nu\alpha_0\mathrm{E}[<n_B>]\,, \\
\frac{d}{dt}\mathrm{E}[<n_A^2>] &= -2\kappa\mathrm{E}[<n_A^2 n_B>] + (2\alpha_0 + 1)\nu\mathrm{E}[<n_A>] \\
&\quad -2\nu\mathrm{E}[<n_A^2>] + \kappa\mathrm{E}[<n_A n_B>] + \nu\alpha_0\,, \\
\frac{d}{dt}\mathrm{E}[<n_B^2>] &= 2\kappa\mathrm{E}[<n_A n_B^2>] - 2(K_b + \nu + \lambda)\mathrm{E}[<n_B^2>] \\
&\quad +2\lambda\mathrm{E}[<n_B>^2] + \kappa\mathrm{E}[<n_A n_B>] \\
&\quad +(K_b + \nu + 2\lambda)\mathrm{E}[<n_B>]\,.
\end{aligned} \tag{8}$$

Equations (6) - (8) contain two sorts of higher-order terms which must be removed to close the system. Firstly, $\mathrm{E}[<n_A><n_B>]$ and $\mathrm{E}[<n_B>^2]$ are second-order moments of $<n_A>$ and $<n_B>$ with respect to the distribution of state variables at time t. In the following we ignore fluctuations in these quantities (also in $\mathrm{E}[<n_A n_B>]$, $\mathrm{E}[<n_A^2>]$ and $\mathrm{E}[<n_B^2>]$), so $\mathrm{E}[<n_A><n_B>] = \mathrm{E}[<n_A>]\,\mathrm{E}[<n_B>]$ and $\mathrm{E}[<n_B>^2] = \mathrm{E}[<n_B>]^2$. It is anticipated that this approximation will be valid for large system size N. Secondly, $\mathrm{E}[<n_A^2 n_B>]$ and $\mathrm{E}[<n_A^2 n_B>]$ are third-order terms with respect to the spatial distribution. These terms will be approximated by functions of the first- and second-order quantities $\mathrm{E}[<n_A>]$, $\mathrm{E}[<n_B>]$, $\mathrm{E}[<n_A n_B>]$, $\mathrm{E}[<n_A^2>]$ and $\mathrm{E}[<n_B^2>]$. Two forms of closure (functional forms), stochastic linearization and the log-Normal approximation are now considered.

A. Stochastic linearization

In this method any terms which are non-linear in *stochastic* variables are removed by replacing carefully selected expressions with their expectations [29]. Equations describing the evolution of the moments of the resulting linear model are closed, and thus can be used to approximate the original nonlinear process. In the present case modifying the site specific autocatalytic reaction rate in (4) to $K\mathrm{E}[<n_A n_B>]$, that is the expectation of the average reaction rate over all sites, leads to a closed system of equations which can be obtained from (6) - (8) by substituting

$$\begin{aligned}
\mathrm{E}[<n_A^2 n_B>] &= \mathrm{E}[<n_A>]\mathrm{E}[<n_A n_B>] \quad \text{and} \\
\mathrm{E}[<n_A n_B^2>] &= \mathrm{E}[<n_A n_B>]\mathrm{E}[<n_B>]\,.
\end{aligned} \tag{9}$$

Under this approximation the covariance $C_{AB} = \mathrm{E}[<n_A n_B>] - \mathrm{E}[<n_A>]\mathrm{E}[<n_B>]$ obeys the equation

$$\begin{aligned}
\frac{d}{dt}C_{AB}(t) &= -(\lambda + \kappa + K_b + 2\nu)C_{AB}(t) \\
&\quad -\kappa\mathrm{E}[<n_A(t)>]\mathrm{E}[<n_B(t)>]\,,
\end{aligned} \tag{10}$$

which may be solved by Fourier transformation and application of the convolution theorem to give

$$\begin{aligned}
C_{AB}(t) = -\kappa\int_0^\infty &\mathrm{E}[<n_A(t-T)>]\mathrm{E}[<n_B(t-T)>] \\
&\times e^{-(\lambda+\kappa+K_b+2\nu)T}dT\,.
\end{aligned} \tag{11}$$

Keeling *et. al* [15] obtain a similar result in the context of predator-prey models, suggesting that it reveals the form of delay equation which would account for spatial heterogeneity in the system. Expression (11) also shows that $C_{AB} \le 0$, so the reaction rate in the spatial model, $K\mathrm{E}[<n_A n_B>] = K\mathrm{E}[<n_A>]\mathrm{E}[<n_B>] + KC_{AB}$, is typically lower than that of the mean field (deterministic) model $K\mathrm{E}[<n_A>]\mathrm{E}[<n_B>]$. The degree of negative correlation quantifies the local depletion of reactants in the spatial system. Further insight comes from examining the steady state solution of the stochastic linearization (6), (7) and (10) for the large mixing limit, $\lambda \to \infty$, where the covariance C_{AB} becomes zero and $\mathrm{E}[<n_A>]$ and $\mathrm{E}[<n_B>]$ correspond to the reactive state of the deterministic system (2). Thus a large degree of mixing reduces the correlations between reactants, reflecting the associated break-down of spatial structure.

Figure 6 shows the results of numerical solution of the stochastic linearization approximation together with a

typical realization of the full stochastic process, shown in Figure 4, for moderate mixing rate $\lambda = 1$. The confidence intervals shown are based on the standard errors

$$\sigma_A = \sqrt{\mathrm{E}[<n_A^2>] - \mathrm{E}[<n_A>]\mathrm{E}[<n_A>]}/\sqrt{N}$$
$$\sigma_B = \sqrt{\mathrm{E}[<n_B^2>] - \mathrm{E}[<n_B>]\mathrm{E}[<n_B>]}/\sqrt{N}\,,$$

and the results show good agreement between simulation and approximation. Moreover, the reactant levels are close to those of the reactive state (α_1, β_1) of the deterministic system (1). In contrast, the situation shown in Figure 7 with $\lambda = 0.01$ demonstrates that the stochastic linearization approximation breaks down for low mixing rates. In this regime Figure 4 shows the reactive state of spatial stochastic process to be unstable, with the system settling down to the unreactive state after a short transient phase. However, stochastic linearization predicts that the steady state reactant levels will shift compared with the case of perfect mixing, but that the reactive state will remain stable. Such failings motivate application of an alternative approximation.

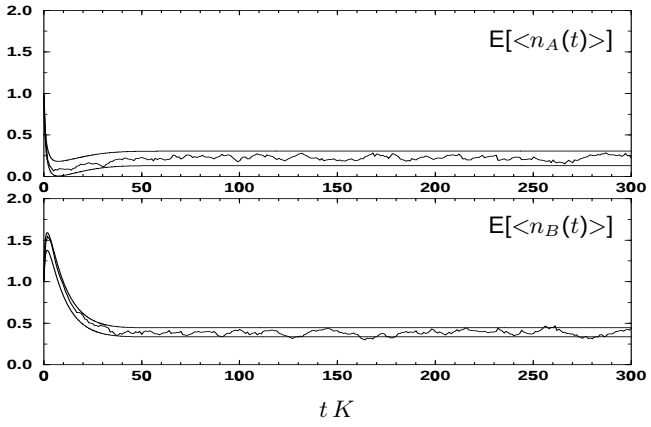

FIG. 6: **Stochastic linearization:** Large mixing rate λ = 1. The top graph shows a typical realization (also shown in Figure 4) of the average density $<n_A(t)>$ against re-scaled time tK from the stochastic spatial autocatalytic process (jagged line). The con dence interval $\mathrm{E}[<n_A>] \pm 1.96\sigma_A$ (solid curves) are obtained by numerical solution of (6)-(8) under the stochastic linearization approximation (9). The bottom graph depicts the same information for reactant B. In each case the parameter values are K = 1, α_0 = 1, K_b = ν = 1/17 and N = 500.

B. Log-Normal approximation

An alternative to stochastic linearization is to make some assumption concerning the distribution of reactant levels over sites. A possible choice is the Gaussian distribution, but in the low mixing regime the average level of reactant B tends to zero, suggesting that this or any other symmetric distribution would be a poor approximation. A non-symmetric alternative is to assume a

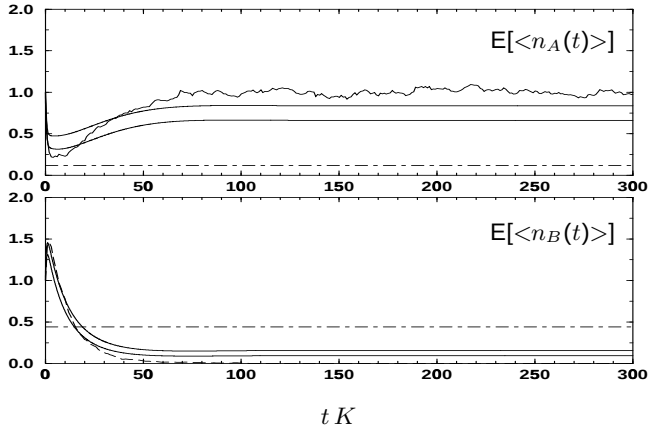

FIG. 7: **Stochastic linearization:** As Figure 6 but for small mixing rate λ = 0.01. The reactive state (α_1, β_1) of the deterministic system (1) is also shown (dot-dashed lines).

log-Normal distribution of reactant levels over sites. As shown in Appendix 1, this enables the third-order terms in the equations (6)-(8) to be approximated by

$$\mathrm{E}[<n_A^2 n_B>] = \frac{\mathrm{E}[<n_A^2>]\mathrm{E}[<n_A n_B>]^2}{\mathrm{E}[<n_A>]^2\mathrm{E}[<n_B>]} \qquad (12)$$
$$\mathrm{E}[<n_A n_B^2>] = \frac{\mathrm{E}[<n_B^2>]\mathrm{E}[<n_A n_B>]^2}{\mathrm{E}[<n_B>]^2\mathrm{E}[<n_A>]}\,.$$

Although the resulting moment evolution equations are more complex than for those associated with stochastic linearization, they nonetheless afford analytic insight. In the large mixing limit, $\lambda \to \infty$, these equations admit to a steady state solution

$$\mathrm{E}[<n_A>] = \mathrm{E}[<n_A^2>] - \mathrm{E}[<n_A>]^2 = (K_b + \nu)/K$$
$$\mathrm{E}[<n_B>] = \mathrm{E}[<n_B^2>] - \mathrm{E}[<n_B>]^2 = \frac{\nu(\alpha_0 K - K_b - \nu)}{(\kappa(K_b + \nu))}$$
$$C_{AB} = 0\,, \qquad (13)$$

which corresponds to a Poisson-like distribution about the deterministic reactive state (2). To first-order as $\lambda \to \infty$, the evolution equation for the correlation C_{AB} becomes

$$\frac{d}{dt}C_{AB}(t) = -\lambda C_{AB}(t)\,.$$

Thus, in this limit the correlation tends to zero exponentially, as mixing breaks down spatial heterogeneity. Furthermore this equation suggests that for $\lambda \to \infty$ the steady state (13) is an attracting state: this conjecture is supported by numerical solution of the log-Normal approximation to the moment evolution equations for $\lambda = 1$, and these results, shown in Figure 8, also demonstrate the accuracy of the log-Normal approximation.

A second steady state of the log-Normal approxima-

tion, valid for all λ is

$$\begin{aligned} \mathrm{E}[<n_A>] &= \alpha_0 \qquad \mathrm{E}[<n_A^2>] - \mathrm{E}[<n_A>]^2 = \alpha_0\,, \\ \mathrm{E}[<n_B>] &= 0 \qquad \mathrm{E}[<n_B^2>] - \mathrm{E}[<n_B>]^2 = 0\,, \\ C_{AB} &= 0\,, \end{aligned} \tag{14}$$

which is a Poisson-like distribution whose mean corresponds to the unreactive state of the deterministic system. Although we have been unable to determine the relative stability of the reactive (13) and unreactive (14) states of the log-Normal approximation analytically, Figure 9 demonstrates that for $\lambda = 0.01$ the unreactive state (14) is asymptotically stable in accord with results obtained by simulation of the full stochastic model shown in Figure 4. Thus, in contrast to stochastic linearization, the log-Normal approximation is able to predict the transition to the unreactive state seen at low levels of mixing.

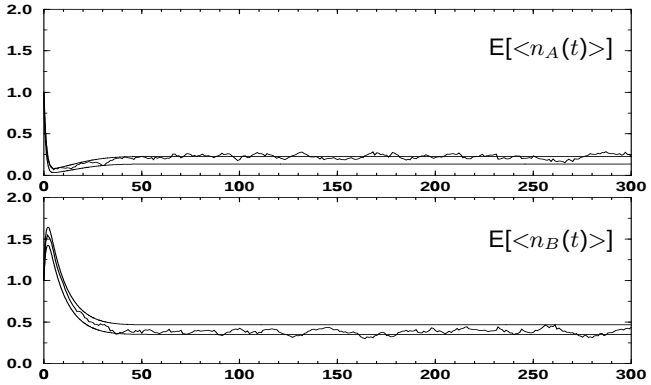

FIG. 8: **Log-Normal approximation:** Large mixing rate λ = 1. The top graph shows a typical realization of the average density $<n_A(t)>$ against re-scaled time tK (jagged line) as shown in Figure 6. The con dence interval $\mathrm{E}[<n_A>] \pm 1.96\sigma_A$ (solid curves) is obtained by numerical solution of (6)-(8) under the log-Normal approximation (12). The bottom graph depicts the same information for reactant B. In each case the parameter values are K = 1, α_0 = 1, K_b = ν = 1/17 and N = 500.

Figure 10 compares the log-Normal approximation with the simulation results of figure 5. The log-Normal approximation is quantitatively correct at the extremes of mixing and no mixing, and although it is less accurate it still captures the qualitative behaviour at intermediate levels of λ. As we have seen in the limit $\lambda \to \infty$, the spatial system becomes well-mixed, and therefore corresponds to the nonspatial system with volume $\Omega = N$. The results of Figures 2 and 10 imply that for small systems ($N < 50$) the reactive state will be unstable for all λ, and the log-Normal approximation will break-down, as is confirmed by direct simulation. This is related to the fact, noted below equations (8), that the moment-closure schemes are expected to be most accurate for large N. This is because we only consider the evolution of the

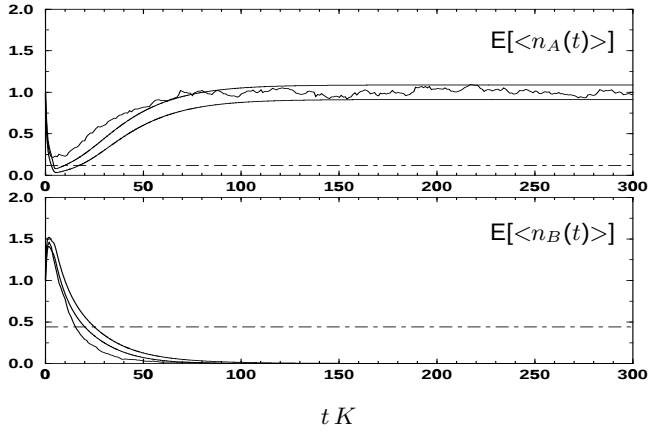

FIG. 9: **Log-Normal approximation:** As Figure 8 but for small mixing rate λ = 0.01. The reactive state (α_1, β_1) of the deterministic system (1) is also shown (dot-dashed lines).

expected values of quantities describing the spatial distribution (i.e. $\mathrm{E}[<n_A>]$, $\mathrm{E}[<n_B>]$, etc.), neglecting any fluctuations between realizations of the process.

Figure 11 shows the corresponding asymptotic behaviour of the covariance and variances in reactant levels across the system for a range of mixing rates. The data shown are from the simulations and solutions to the log-Normal approximation used in Figure 10. The reactants are maximally separated, and thus spatial heterogeneity at its greatest, at the critical mixing rate where the reaction state becomes stable/unstable. For larger mixing rates the correlation increases with λ.

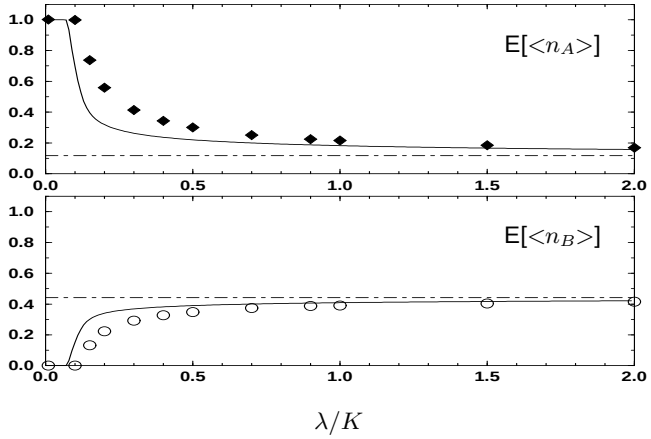

FIG. 10: **Stability of reaction state:** The solid lines show the asymptotic values of $\mathrm{E}[<n_A>]$ and $\mathrm{E}[<n_B>]$ (as indicated) obtained from the solution of the log-Normal approximation for a range of relative mixing rates λ/K. The symbols represent estimates of $\mathrm{E}[<n_A>]$ (diamonds) and $\mathrm{E}[<n_B>]$ (circles) obtained from 10 simulation runs, with samples collected, after a burn-in period, from t = 500, ..., 1000. The standard errors in these estimates are approximately equal to the size of the symbols. The parameter values are K = 1, α_0 = 1, K_b = ν = 1/17 and N = 500.

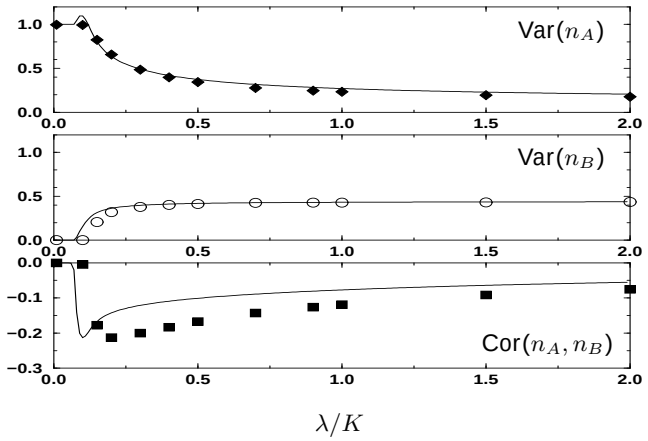

FIG. 11: **Stability of reaction state:** The solid lines show the asymptotic values of Var(n_A) = E[$<n_A^2>$] − E[$<n_A>$]^2, Var(n_B) = E[$<n_B^2>$] − E[$<n_B>$]^2 and the normalized correlation Cor(n_A, n_B) = $C_{AB}/\sqrt{\text{Var}(n_A)\text{Var}(n_B)}$ (as indicated) obtained from solution of the log-Normal approximation for a range of values of the relative mixing rate λ/K. The symbols represent estimates of E[Var(n_A)] (diamonds), E[Var(n_B)] (circles) and E[Cor(n_A, n_B)] (squares) obtained from 10 simulation runs, with samples collected after a burn-in period from t = 500, ..., 1000. The standard errors in these estimates are approximately equal to the size of the symbols. The parameter values are K = 1, α_0 = 1, K_b = ν = 1/17 and N = 500.

IV. DISCUSSION

A living cell is an open system, which can communicate with environments by transferring chemical signals and energy. Enzymatic reactions in living cells are confined to very small spatial volumes. Moreover, these reactions are subject to strong thermal fluctuations inside the cells due to a flow of energy [14], and these conditions can lead to qualitative changes in the kinetics of enzymatic reactions in comparison with high-density well mixed conditions. For example, coherent dynamics can form between substrates and enzymes when the reaction takes place in small volumes [14, 30–32]. Furthermore, our results suggest that without sufficient communication between cells certain biochemical reactions might be unstable with respect to thermal fluctuations. It would also be interesting to study the effects of within-cell spatial heterogeneity. In living cells, a large number of enzymatic reactions are networked in complicated ways, and are coupled to thousands of substrates. Pathways can be unidirectional, reversible, branched, or cyclic, and there are many different types of inhibition and activation [33]. In the post genome era, these complex networks can be reconstructed based on genomic data. Unsurprisingly, the purposes and functions of complex biochemical networks, in particular spatio-temporal self-organization behaviour, has attracted much attention [34, 35]. For enzymatic reactions, various mechanisms may lead to spatio-temporal behaviour [36]. Autocatalysis represents a class of reactions of great importance to living cells and has been much studied in nonspatial contexts [2, 3, 5, 6]. Togashi and Kaneko [37] show that stochastic fluctuations and discreteness in molecular numbers leads to transitions between states in a nonspatial autocatalytic system. The stochastic spatio-temporal autocatalytic process studied in this work can be considered a generic model for studying spatio-temporal behaviour in biochemical reactions. We note that Velikanov and Kapral [38] study the propagation of traveling wave fronts in a spatially explicit discrete time (Markov Chain) model of quadratic autocatalysis. Using a perturbation technique, which systematically accounts for spatial correlations, they show that the wave front velocity of the stochastic system is lower than that predicted by a mean-field analysis which ignores such correlations. Moreover, as the diffusion coefficient increases spatial correlations are minimized and the discrepancy reduced. The phenomenon is analogous to the effect of finite mixing on the stability of the reactive state explored in the current paper. The model studied here was amenable to a spatial moment-closure approximation which compared favourably with simulations of the full stochastic process; these results demonstrate the utility of order-parameters, such as the spatial averages considered here, in studying system behaviour. Our investigations clearly show how internal fluctuations, small volumes and heterogeneity affect the kinetics of the quadratic catalytic system.

In the nonspatial system at low volumes, the reactive state of the autocatalytic process is unstable to internal stochastic fluctuations. The spatial model shows that such unstable components can be linked together, via random exchange of reactants, to form a system in which the reaction is stable. For large mixing rate ($\lambda \to \infty$) the spatial system with N components behaves like a nonspatial system with volume N, but for finite mixing rate this effective volume is less than N. Thus, finite mixing generates spatial heterogeneity (correlation) which destabilizes the system with respect to a perfectly mixed system of the same volume, and there is a critical level of exchange (mixing) below which the reaction is unstable. Conversely, at the level of the cell, finite mixing stabilizes the reaction kinetics by forming a system whose effective volume is much greater than any individual cell. In conclusion, our results suggest that autocatalytic reaction kinetics may only be stable in cellular systems in which a number of cells are able to exchange reactants via some transport process. Perhaps such phenomena influenced evolution by favouring the persistence of aggregations of multiple cells over that of solitary individuals.

Appendix: Log-Normal approximation

If the reactant levels n_A and n_B are log-Normally distributed over sites, then $y_1 = \log n_A$ and $y_2 = \log n_B$ are

joint Normal with m.g.f. (Kendall, 1994)

$$M(\theta_1,\theta_2) \equiv \mathrm{E}[<\exp\{\theta_1 y_1 + \theta_2 y_2\}>] = \exp\{\kappa_{10}\theta_1 + \kappa_{01}\theta_2 + \kappa_{20}\theta_1^2/2 + \kappa_{11}\theta_1\theta_2 + \kappa_{02}\theta_2^2/2\},$$

where $\mathrm{E}[<\,.\,>]$ denotes the expectation over distributions in space and time, and

$$\begin{aligned}
\kappa_{10} &= 2\log(\mathrm{E}[<n_A>]) - \log(\mathrm{E}[<n_A^2>])/2\,,\\
\kappa_{01} &= 2\log(\mathrm{E}[<n_B>]) - \log(\mathrm{E}[<n_B^2>])/2\\
\kappa_{20} &= \log(\mathrm{E}[<n_A^2>]) - 2\log(\mathrm{E}[<n_A>])\,,\\
\kappa_{02} &= \log(\mathrm{E}[<n_B^2>]) - 2\log(\mathrm{E}[<n_B>])\\
\kappa_{11} &= \log(\mathrm{E}[<n_A n_B>]) - (\kappa_{20}+\kappa_{02})/2 - \kappa_{10} - \kappa_{01}\,.
\end{aligned}$$

For appropriate choice of θ_1 and θ_2 expressions for the higher-order terms $\mathrm{E}[<n_A^2 n_B>]$ and $\mathrm{E}[<n_A n_B^2>]$ are obtained from

$$\mathrm{E}[<n_A^{\theta_1} n_B^{\theta_2}>] = <[\exp\{\theta_1 y_1 + \theta_2 y_2\}> = M(\theta_1,\theta_2)\,.$$

For example setting $\theta_1 = 2$ and $\theta_2 = 1$ yields

$$\begin{aligned}
\mathrm{E}[<n_A^2 n_B>] &= M(2,1)\\
&= \exp\{2\kappa_{10} + \kappa_{01} + 2\kappa_{20} + 2\kappa_{11} + \kappa_{02}/2\}\,,
\end{aligned}$$

which simplifies to

$$\mathrm{E}[<n_A^2 n_B>] = \frac{\mathrm{E}[<n_A^2>]\mathrm{E}[<n_A n_B>]^2}{\mathrm{E}[<n_A>]^2\mathrm{E}[<n_B>]}\,.$$

The resulting expressions (12) can then be used to close the system of moment evolution equations (6)-(8).

Acknowledgments

The authors would like to thank the BBSRC and EPSRC (UK) for their financial support under Grant 78/MMI09712, and three anonymous referees for their useful comments. In addition, GM and JL gratefully acknowledge the support of the Scottish Executive Environment and Rural Affairs Department.

[1] M. A. Gibson and J. Bruck, in *Computational modeling of genetic and biochemical networks*, edited by J. M. Bower and H. Bolouri (Massachusetts Institute of Technology Press, Cambridge, MA, 2001).
[2] P. Gray and S. K. Scott, Chem. Engng Sci. **39**, 1087 (1984).
[3] P. Gray and S. K. Scott, *Chemical oscillations and instabilities* (Oxford University Press, Oxford, UK, 1990).
[4] A. Goldbeter, *Biochemical Oscillations and Cellular Rhythms: the molecular basis of periodic and chaotic behaviour* (Cambridge University Press, Cambridge, UK, 1996).
[5] J. Liu and J. W. Crawford, Proc. Roy. Soc. Lond., A **453**, 1195 (1997).
[6] J. Liu and S. K. Scott, J. Chem. Phys. **94**, 4416 (1991).
[7] W. Horsthemke and R. Lefever, *1984* (Springer-Verlag, Berlin, 1984).
[8] G. Marion, X. Mao, E. Renshaw, and J. Liu, In preparation (2002).
[9] N. G. Van Kampen, *Stochastic Processes in Physics and Chemistry* (North Holland, Amsterdam, 1992).
[10] E. Renshaw, *Modelling Biological Populations in Space and Time* (Cambridge University Press, Cambridge, UK, 1991).
[11] M. Malek Mansour, C. Van den Broeck, G. Nicolis, and J. W. Turner, Ann. Phys. **131**, 283 (1981).
[12] K. Kitahara, Adv. Chem. Phys. **29**, 85 (1975).
[13] Q. Zheng, J. Ross, K. L. C. Hunt, and P. M. Hunt, J. Chem. Phys. **96**, 630 (1992).
[14] B. Hess and A. S. Mikhailov, Science **264**, 223 (1994).
[15] M. J. Keeling, H. B. Wilson, and P. S. W., Science **290**, 1758 (2000).
[16] M. J. Keeling, J. Anim. Ecol. **69**, 725 (2000).
[17] V. Isham, Math. Biosci. **107**, 209 (1991).
[18] G. Marion, E. Renshaw, and G. Gibson, Theor. Pop. Biol. **57**, 197 (2000).
[19] P. Whittle, J. Roy. Statist. Soc. B **19**, 266 (1957).
[20] J. H. Matis, T. R. Ki e, and P. P. R., Theor. Popul. Biol. **53**, 16 (1998).
[21] J. H. Matis and T. R. Ki e, *Stochastic Population Models:Lecture Notes in Statistics 145* (Springer, New York, 2000).
[22] M. G. Kendall, *Kendall's Advanced Theory of Statistics* (Edward Arnold, London, 1994).
[23] E. Renshaw, Math. Biosci. **168**, 57 (1999).
[24] S. A. Levin and R. Durrett, Phil. Trans. Roy. Soc. Lond. B **351**, 1615 (1996).
[25] B. Bolker and S. W. Pacala, Theor. Pop. Biol. **52**, 179 (1997).
[26] J. A. N. Filipe and G. J. Gibson, Phil. Trans. Roy. Soc. Lond. B **353**, 2153 (1998).
[27] E. Ben-Naim and P. L. Krapivsky, J. Phys. A **27**, L481 (1994).
[28] A. Kostyuk, M. Gorenstein, H. Stocker, and W. Grenier, Phys. Rev. C. **63**, art. no. 044901 (2001).
[29] W. Y. Tan and H. Hsu, Stat. Med. **8**, 121 (1989).
[30] B. Hess and A. S. Mikhailov, Biophys. Chem. **58**, 365 (1996).
[31] P. Stange, A. S. Mikhailov, and B. Hess, J. Phys. Chem. B. **103**, 6111 (1999).
[32] P. Stange, A. S. Mikhailov, and B. Hess, J. Phys. Chem. B. **104**, 1844 (2000).
[33] L. Stryer, *Biochemistry* (W. H. Freeman and Company, New York, 1991).
[34] A. C. Moller, M. J. B. Hauser, and L. F. Olsen, Biophys. Chem. **72**, 63 (1998).

[35] M. J. Berridge, Nature **386**, 759 (1997).
[36] I. Schreiber, Y. F. Hung, and J. Ross, J. Phys. Chem. **100**, 8556 (1996).
[37] Y. Togashi and K. Kaneko, Phys. Rev. Lett. **86**, 2459 (2001).
[38] M. V. Velikanov and R. Kapral, J. Chem. Phys. **110**, 109 (1999).